nature
COMMUNICATIONS

ARTICLE

Topological states in multi-orbital HgTe honeycomb lattices

W. Beugeling[1], E. Kalesaki[2,3], C. Delerue[2], Y.-M. Niquet[4,5], D. Vanmaekelbergh[6] & C. Morais Smith[7]

Research on graphene has revealed remarkable phenomena arising in the honeycomb lattice. However, the quantum spin Hall effect predicted at the K point could not be observed in graphene and other honeycomb structures of light elements due to an insufficiently strong spin–orbit coupling. Here we show theoretically that 2D honeycomb lattices of HgTe can combine the effects of the honeycomb geometry and strong spin–orbit coupling. The conduction bands, experimentally accessible via doping, can be described by a tight-binding lattice model as in graphene, but including multi-orbital degrees of freedom and spin–orbit coupling. This results in very large topological gaps (up to 35 meV) and a flattened band detached from the others. Owing to this flat band and the sizable Coulomb interaction, honeycomb structures of HgTe constitute a promising platform for the observation of a fractional Chern insulator or a fractional quantum spin Hall phase.

[1] Max-Planck-Institut für Physik komplexer Systeme, Nöthnitzer Straße 38, 01187 Dresden, Germany. [2] IEMN-Department ISEN, UMR CNRS 8520, 41 Boulevard Vauban, 59046 Lille, France. [3] Physics and Materials Science Research Unit, University of Luxembourg, 162A Avenue de la Faïencerie, L-1511 Luxembourg, Luxembourg. [4] Université Grenoble Alpes, INAC-SP2M, L_Sim, 17 avenue des Martyrs, 38054 Grenoble, France. [5] CEA, INAC-SP2M, L_Sim, 17 avenue des Martyrs, 38054 Grenoble, France. [6] Debye Institute for Nanomaterials Science, Utrecht University, Princetonplein 1, 3584 CC Utrecht, The Netherlands. [7] Institute for Theoretical Physics, Center for Extreme Matter and Emergent Phenomena, Utrecht University, Leuvenlaan 4, 3584 CE Utrecht, The Netherlands. Correspondence and requests for materials should be addressed to C.D. (email: christophe.delerue@isen.fr) or to C.M.S. (email: C.deMoraisSmith@uu.nl).

The discovery of graphene has confronted us with a material that exhibits fascinating electronic properties[1], such as zero-mass carriers, persisting conductivity at vanishing density at the Dirac point[2], Klein tunnelling[3] and an anomalous quantum Hall effect[4–6]. Nevertheless, the absence of a bandgap in its spectrum prevents its use as a field-effect transistor, and its weak spin–orbit coupling (SOC) hampers the possibility to realize the quantum spin Hall effect (QSHE)[7] and use it for quantum spintronics. The prospect of artificial graphene samples[8] that display the lacking properties has motivated research in various types of honeycomb lattice, such as arrays of ultracold atoms[9], molecular graphene[10], organometallic lattices[11] and two-dimensional (2D) electron gases subject to a geometric array of gates[12,13]. Recently, an alternative path came from the self-assembly of semiconductor nanocrystals forming atomically coherent 2D structures with a long-range honeycomb pattern; the thickness and honeycomb period are defined by the size of the nanocrystals, which is in the range of 5 nm (refs 14,15). Honeycomb lattices of PbSe and CdSe nanocrystals have been fabricated, with astonishing atomic coherence due to the oriented attachment of the nanocrystals. Theoretical investigations have shown that CdSe superlattices formed in such a way exhibit Dirac cones at two energies and nearly dispersionless bands. Unfortunately, these flat bands are connected to the nearby higher energy bands, and the SOC gaps in the conduction band are very small[16].

In this work, we propose a design for robust topological insulators that combine the properties of the honeycomb lattice and strong SOC. We consider three different types of HgTe layers with superimposed honeycomb geometry and present atomistic tight-binding (TB) calculations of their conduction band structure that we accurately describe by a 16-band effective model. Such lattices take advantage of the multi-orbital degrees of freedom in the honeycomb setup, allied to the strong SOC[17]. The access to multi-orbital degrees of freedom allows for further manipulation of the topological properties. While the Haldane[18] and Kane–Mele[7] models originally concerned honeycomb lattices characterized by a single orbital per site (for example, p_z in graphene) and isotropic nearest-neighbour (NN) hopping integrals between them, multi-orbital models have attracted much attention recently, in particular because they seem to be a paradigm to generate topologically non-trivial flat bands[19–23]. The flat band structure opens the way to the realization of interesting strongly correlated states, such as fractional QSHE, fractional Chern insulators or ferromagnetic fractional Chern insulators[20,22,24–31]. The currently proposed HgTe lattices exhibit conduction bands characterized by large topological gaps and an isolated flat band. We conclude that, depending on the position of the Fermi level, not only QSHE could be observed in these structures, but also fractional QSHE or fractional Chern insulator phases, as on-site and NN Coulomb-interaction parameters are found in the energy range required for their realization.

Results

Design of the HgTe honeycomb lattices. The three structures that we consider have in common that the [111] direction of the zincblende lattice is perpendicular to the plane. The first system is inspired by recent results obtained for nanocrystal self-assembly[14,15], that is, a graphene-type superlattice of truncated cubic nanocrystals attached via ⟨110⟩ facets. The second system consists of spheres connected by short cylinders, which allow us to vary the coupling between honeycomb lattice sites in a convenient way. The third system corresponds to a honeycomb array of cylinders. These two last systems may be experimentally realized by gas-phase deposition and lithography. We will show below

that the multi-orbital topological effects are common to these three different structures.

The HgTe superlattices proposed here differ fundamentally from HgTe/CdTe quantum wells, where the QSHE has been predicted[32] and experimentally observed[33]. In the latter system, the appearance of the QSHE at the Γ point is connected to band inversion and vanishes for quantum wells of thickness below 6 nm. Here instead, the effect occurs at the K point, and it is driven by the honeycomb nanogeometry, allied to the strong SOC of the composing HgTe nanocrystals. This distinction is important because zero modes (Majoranas) bind to topological lattice defects when the bandgap opens at a non-Γ point in the Brillouin zone[34,35], and hence, the underlying topological order can be detected by measuring the structure of the topological defect[36,37].

Band structure of lattices of HgTe nanocrystals. To unveil the topological properties of these systems, we have performed atomistic TB band structure calculations. We use a basis of 20 atomic orbitals on each atom of the nanocrystals, including the spin degree of freedom. The methodology is described in ref. 38 and is summarized in the Methods section. In comparison with bulk HgTe, the electronic structure of HgTe superlattices is characterized by a large bandgap due to the strong quantum confinement. Conduction and valence bands close to this gap are composed of several minibands and minigaps due to the periodic scattering of the electronic waves in the honeycomb structure[16]. In the following, we only discuss the physics of the sixteen lowest conduction bands (Fig. 1).

A typical honeycomb lattice composed of HgTe nanocrystals is shown in Fig. 1a and the related conduction band structure is displayed in Fig. 1c. To visualize the effects of SOC, we compare it with the band structure of the same honeycomb structure composed of CdSe (Fig. 1b). The strong SOC in HgTe gives rise to effects which are absent in CdSe[16]. The overall behaviour of the band structure can be understood as follows. Each individual nanocrystal is characterized by two states with s envelope wavefunction and six p states at higher energy. In the honeycomb structure, strong coupling between the wavefunctions of neighbour nanocrystals leads to the formation of 16 bands grouped into two manifolds of four (s) and 12 (p) bands that are well separated. The s bands have the same type of dispersion as the π and $\pi^\star$ bands in real graphene[1]. In the case of CdSe (Fig. 1b), these bands are spin degenerate and are connected at the K and K′ points of the Brillouin zone, where their dispersion is linear (Dirac points). In HgTe, instead, the s bands exhibit a small gap (5.7 meV) at the K points and have a quadratic dispersion (see Fig. 1c). In addition, they are characterized by a visible spin splitting at all points of the Brillouin zone, except at Γ and M. Among the 12 p bands of CdSe nanocrystal superlattices, eight have a small dispersion and the other four basically behave like the (Dirac) s bands. Four flat bands are built from the p_z states perpendicular to the lattice, which are not very dispersive because p_z–p_z (π) interactions are weak. Four other bands ($p_{x,y}$), respectively above and below the p Dirac band, are flat due to destructive interferences of electron hopping induced by the honeycomb geometry[19,20]. In honeycomb lattices of HgTe nanocrystals, the SOC induces spin splitting, opens a large gap at K in the p-like Dirac bands, and produces a considerable detachment of the lowest flat p band from the Dirac p band (Fig. 1c). The effects of the SOC are so strong that it is hardly possible to recognize the Dirac bands.

These unexpected features allow for the realization of several topological states of matter, by doping the system using a field-effect transistor or electrolyte gel gating[39]. At zero energy, the
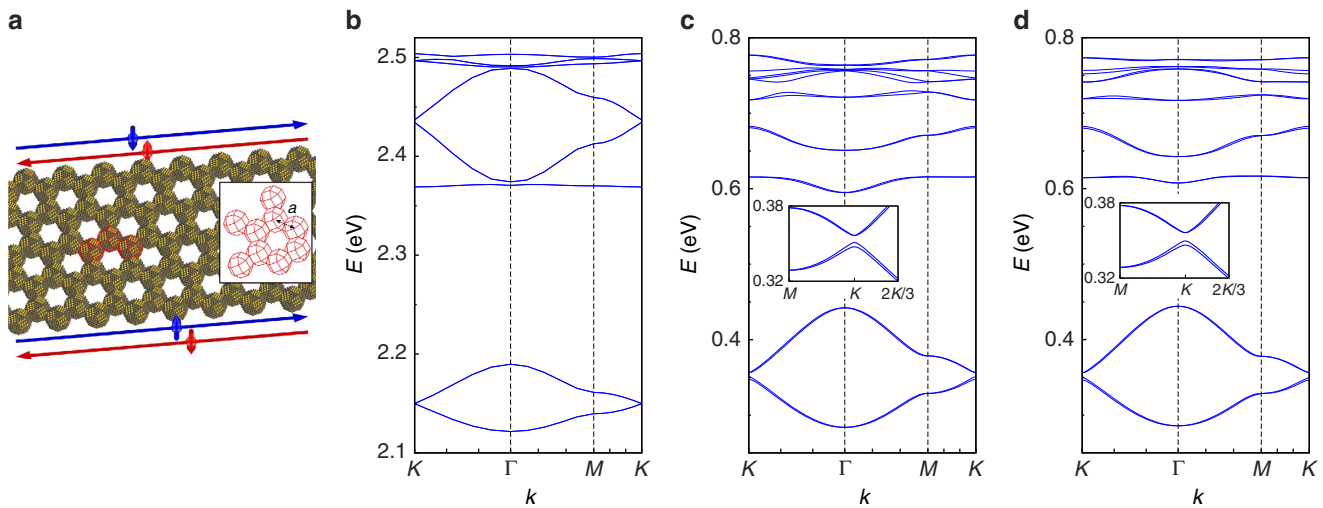
Figure 1 | Nanocrystal lattices and their conduction band dispersions. (**a**) honeycomb nanoribbon formed by the HgTe (CdSe) nanocrystals. Hg (Cd) atoms are in yellow, Te (Se) atoms are in grey. Each nanocrystal has a truncated nanocube shape, the vertices of which are given by all permutations of $[\pm 1, \pm(1-q), \pm(1-q)]l$, where q is the truncation factor and $2l$ is the size of the original nanocube before truncation. The honeycomb lattice spacing a, that is, the centre-to-centre distance between neighbor nanocrystals, is defined as $a = (2N+1)a_0/\sqrt{2}$ where N is an integer and a_0 is the cubic lattice parameter of HgTe (CdSe). The nanocrystals are attached via $\langle 110\rangle$ facets ($a = \sqrt{2}(2-q)l$). The arrows along the ribbon indicate the electron propagation in the helical edge states present in the quantum spin Hall phase. Red and blue colours correspond to top and bottom edge for spin up, bottom and top edge for spin down, respectively. (**b,c**) Band dispersions for the bulk resulting from the atomistic TB calculations with $q = 0.5$ ($a = 5.0$ nm for HgTe, 4.7 nm for CdSe). (**d**) Same for the HgTe superlattice resulting from the effective model. Insets in **c,d** show the s bands in the gap region with higher magnification $\left[2K/3 = \left(\frac{4\pi}{9a}, \frac{4\pi}{9\sqrt{3}a}\right)\right]$.

undoped system is a semiconductor with a trivial gap of about 0.4 eV. On doping the material with one electron per nanocrystal, the small s-like topological gap may be reached, whereas for fillings between two and three electrons per nanocrystal, the fractional quantum (spin) Hall regime may be realized at the flat band. For a doping level of four electrons per nanocrystal, one reaches the QSHE gap. At this point, we should emphasize that doping of nanocrystals with up to 10 electrons has already been demonstrated experimentally[40]; therefore, all the interesting regimes that we discuss are at reach with the existing technology, at a simple switch of the doping level. Other examples of band structures for lattices of HgTe nanocrystals with different size or truncation factors are presented in Supplementary Fig. 1 and are discussed in Supplementary Note 1. They all show large topological gaps, especially in the p sector.

The topological properties of the bands are most transparently studied through an edge-state analysis in a one-dimensional nanoribbon[41]. We consider a zigzag ribbon composed of 16 nanocrystals (34,740 atoms) per unit cell. Figure 2a shows that edge states are crossing the three gaps between the p bands as well as the gap between the s bands. These results also hold for armchair ribbons. In Supplementary Fig. 2a and Supplementary Note 2, we present the band structure for another nanoribbon, which has two inequivalent edges. Still, helical edge states characteristic of the QSHE are found, as shown by the 2D plots of the wavefunctions (Supplementary Figs 2b–e).

Effective model. The band structures resulting from the atomistic TB calculations are accurately described by a 16-band effective model (Fig. 1d), where each nanocrystal is treated as one site on a honeycomb lattice. The effective TB model is written in the basis of the four aforementioned orbitals (s, p_x, p_y, p_z) per site as $H_{eff} = H_\mu + H_{NN} + H_{ISO} + H_{RSO}$. Here H_μ incorporates the on-site energies E_s, $E_{p_x} = E_{p_y}$, and E_{p_z}. The edge nanocrystals have a

slightly different value of E_s compared with the bulk, to account for the different number of neighbours. The term

$$H_{NN} = \sum_{\langle i,j\rangle} \sum_{\substack{\alpha \\ b,b'}} c^\dagger_{i,b,\alpha} V_{i,b;j,b'} c_{j,b',\alpha},\qquad(1)$$

encodes NN hopping, where $\langle i,j\rangle$ denotes NN sites, $\alpha = \uparrow, \downarrow$ denotes spin and b and b' the orbitals. The coupling coefficients $V_{i,b;j,b'}$ are expressed in terms of the hopping parameters $V_{ss\sigma}$, $V_{pp\sigma}$, $V_{pp\pi}$ and $V_{sp\sigma}$, following the notations of ref. 42.

The intrinsic SOC term H_{ISO} couples the electron orbital angular momentum $\mathbf{L}$ and spin $\mathbf{S} = \sigma/2$. In the p sector, it is encoded through the on-site term $\lambda^p_{ISO}\mathbf{L}\cdot\sigma$. There is no on-site term in the s sector because the orbital angular momentum is 'frozen'. For the same reason, in graphene, the on-site intrinsic SOC term is absent because the sp^2 hybridization freezes the orbital momentum in the p_z state. However, as shown by Kane and Mele[7], the intrinsic SOC introduces a next-NN (NNN) hopping term, which is written as

$$H_{ISO} = i\lambda^s_{ISO} \sum_{\langle\langle i,j\rangle\rangle} \sum_\alpha c^\dagger_{i,s,\alpha} \sigma^z_{\alpha\alpha} v_{ij} c_{j,s,\alpha}.\qquad(2)$$

Here the summation is over NNNs, and $v_{ij} = \pm 1$, with the sign depending on the outer product of the two NN vectors that connect sites i and j. The Rashba SOC term, proportional to the cross product of momentum and spin, $\mathbf{p}\times\mathbf{S}$, is written as an NN hopping term

$$H_{RSO} = i \sum_{\langle i,j\rangle} \sum_{\substack{\alpha,\beta \\ b,b'}} c^\dagger_{i,b,\alpha} \gamma_{i,b;j,b'} \left[\hat{z}\cdot(\sigma\times\mathbf{r}_{ij})\right]_{\alpha\beta} c_{j,b',\beta}.\qquad(3)$$

The coupling coefficients $\gamma_{i,b;j,b'}$ have the same structure as the $V_{i,b;j,b'}$ for the ordinary NN hopping and are expressed in terms of $\gamma_{ss\sigma}$, $\gamma_{pp\sigma}$ and $\gamma_{pp\pi}$. The sp term may be neglected due to the large energy separation between the s and p bands.
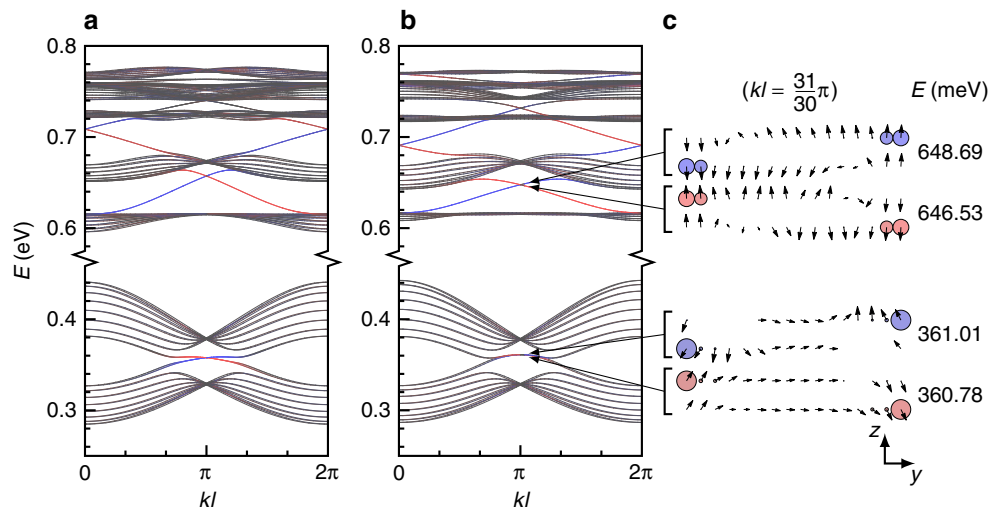
Figure 2 | Topological edge states and non-trivial gaps in honeycomb lattices of HgTe nanocrystals. (**a**) Conduction bands calculated using the atomistic TB method for a zigzag ribbon composed of 16 nanocrystals per unit cell ($q = 0.5$, body diagonal of 5.0 nm, cell length $l = 8.7$ nm). (**b**) Same but computed from the effective Hamiltonian. (**c**) Spin orientation on each site for a selection of states calculated at $k = 31\pi/(30l)$. A vertical arrow indicates that the spin is along the z direction, perpendicular to the lattice. The size of the circles represents the weight of the wavefunction on each site. In each figure, the colour indicates the expectation value $\langle y\sigma_z \rangle$, that is, red and blue correspond to top and bottom edge for spin up (bottom and top edge for spin down), respectively. At each energy E, there are two states that live on opposite edges with opposite spin; therefore, they are represented by the same colour. The bulk states are grey.

In Table 1, we present typical values for the parameters obtained numerically using least-squares fitting to the band structure of Fig. 1c. The band structure of the effective model is shown in Fig. 1d. As expected, the on-site term λ_{ISO}^p is much larger than the NNN term λ_{ISO}^s, explaining the opening of a very large gap at the K point and the detachment of the flat bands in the p sector. Using the effective model, the non-trivial topology of the bands is confirmed by the calculation of the Z_2 topological invariant, the spin Chern number (Methods).

The effective model yields a band structure for the ribbon (Fig. 2b) in excellent agreement with the atomistic TB calculations (Fig. 2a). The red and blue colours in Fig. 2a,b indicate the expectation value $\langle y\sigma_z \rangle = \langle \psi_i | \hat{y}\hat{\sigma}_z | \psi_i \rangle$, where y is the coordinate perpendicular to the ribbon edges. This expectation value allows us to identify helical edge states that come in pairs with identical dispersion, opposite spin, and live on opposite edges. Both atomistic and effective TB models show that the gaps in the s and p sectors exhibit helical edge states, characteristic of the QSHE.

When the Rashba coupling is neglected in the effective model, all states are spin degenerate. The Rashba term induces a small splitting in energy, and tilts the spins slightly away from the perpendicular direction. In Fig. 2c, we plot the spin direction on each site of the zigzag ribbon for four sets of four edge states (two in each edge). The spin direction is always perpendicular to the edge, that is, the spin lies in the yz plane if we choose the x direction to be parallel to the edge. The localization of the selected states on the edges is visible from the weight of the wavefunction, indicated by the size of the circles in the figure. The colours of the circles are determined by the local value of $y\sigma_z$, and correspond to the colours in the dispersion (Fig. 2a,b). The site dependence of the spin direction leads to interesting spin textures. For the edge states, the typical spin texture is almost smooth: Going from one edge to the other, the spin direction interpolates between (almost) up and (almost) down in a rotational manner. A slight tilt of $\sim 3°$ is observed for the edge states in the p bands. In the s bands, the tilt is stronger, similarly to graphene[41]. Here the spin vector at the edge site points $\sim 30°$ away from the vertical. This difference in tilt can be explained by the much larger intrinsic SOC in the p

Table 1 | Parameters of the effective model.

On-site	NN hopping	Rashba SOC	Intrinsic SOC
$E_s^{bulk} = 0.365$ eV	$V_{ss\sigma} = -26.4$ meV	$\gamma_{ss\sigma} = 0.56$ meV	$\lambda_{ISO}^s = 0.71$ meV
$E_s^{edge} = 0.370$ eV	$V_{pp\sigma} = 45.6$ meV	$\gamma_{pp\sigma} = 1.50$ meV	$\lambda_{ISO}^p = 15.8$ meV
$E_{p_x} = 0.691$ eV	$V_{pp\pi} = -2.7$ meV	$\gamma_{pp\pi} = 0.80$ meV	
$E_{p_y} = 0.691$ eV	$V_{sp\sigma} = 31.1$ meV		
$E_{p_z} = 0.747$ eV			

Parameters derived for the lattice of HgTe nanocrystals described in Fig. 1. E_s, E_{p_x}, E_{p_y} and E_{p_z} are the on-site energies on the s, p_x, p_y and p_z orbitals, respectively. In ribbons, the edge nanocrystals have a slightly different value of E_s compared with the bulk ($E_s^{bulk} \neq E_s^{edge}$). $V_{ss\sigma}$, $V_{pp\sigma}$, $V_{pp\pi}$ and $V_{sp\sigma}$ are the hopping parameters, following the notations of ref. 42. $\gamma_{ss\sigma}$, $\gamma_{pp\sigma}$ and $\gamma_{pp\pi}$ are the terms describing the Rashba SOC, following the same notations. The intrinsic SOC is defined by λ_{ISO}^s and λ_{ISO}^p on s and p orbitals, respectively.

sector than in the s one, whereas the two Rashba couplings $\gamma_{ss\sigma}$ and $\gamma_{pp\sigma}$ are of similar order of magnitude. Strictly speaking, one should denote this state a Z_2 topological insulator, but since the Rashba SOC is extremely small, one can think of an approximate QSHE.

Flat band and Coulomb interactions. The large gaps in the p sector are mainly due to the intrinsic SOC, which, contrarily to the Kane-Mele model, is described by an on-site term ($\lambda_{ISO}^p = 15.8$ meV). In particular, the intrinsic SOC separates the lowest flat band from the other p bands, with large gaps, for example, 35 meV in the case of Fig. 1c. This gap ranges from 13 to 36 meV when we vary the nanocrystal size and shape (Supplementary Table 1).

Under partial filling of the lowest-energy flat p band by electrons, fascinating phenomena such as fractional QSHE are predicted in the presence of strong correlations, when the strength of Coulomb interactions between electrons is large compared with the bandwidth and smaller or comparable to the energy gap between the flat band and the next higher one (for a recent review, see ref. 31). In addition, it has been shown that also for large Coulomb interactions, a fractional Chern insulator phase cannot

be ruled out[43]. We have thus calculated the on-site (U) and NN (V) electron–electron interaction energies for the honeycomb lattice of Fig. 1a, assuming two different dielectric environments around the nanocrystals (Methods). Table 2 shows that Coulomb energies are larger than the bandwidth and are comparable to the gap between p bands. Therefore, the gap sizes open the possibility to the experimental observation of strongly correlated quantum phases including the long sought fractional QSHE[20,24–27].

Band structure for other types of HgTe lattices. To understand the effects of the electronic coupling between honeycomb lattice sites, we have studied a second type of superlattices with a simpler geometry, consisting of tangent spheres connected by horizontal cylinders (Fig. 3a,b). The HgTe spheres have their [111] axis orthogonal to the lattice plane and the cylinders are oriented along ⟨110⟩ directions perpendicular to [111]. Figure 3c,d,e

depicts the evolution of the band structure with the ratio between the diameters of cylinders (d) and spheres (D) (see also Supplementary Fig. 3). An increase of d/D induces larger NN hopping terms, broader s and p bands and stronger sp hybridization, as shown by the deformation of the s band. It also results in a larger NNN term λ^s_{ISO}, explaining why the non-trivial gap in the s sector only exists for $d/D > 0.3$. On the contrary, topological gaps are always present in the p sector, even for small values of d/D, because they are mainly determined by the on-site term λ^p_{ISO}. At high values of d/D (>0.7), the spin splitting of the bands in the entire Brillouin zone becomes particularly important due to increased Rashba couplings. In general, the lowest p band is rather flat and has a maximum separation from the next higher one for d/D close to 0.4–0.5. In that case, the energy separation can be as large as 35 meV (Fig. 3f). HgTe honeycomb structures with moderate coupling between lattice sites should provide the most suitable gap and band widths to observe the strongly correlated phases associated to the flatness of the bands.

In Supplementary Fig. 4, we show further results for a third type of honeycomb structure made of overlapping HgTe cylinders parallel to each other. Once again, the band structure can be described by the effective model (Supplementary Note 3, Supplementary Table 2 and Supplementary Fig. 5). In that case, the NN couplings are even stronger, there is no gap in the s sector due to a large Rashba term, but the non-trivial gap above the lowest p band remains. We can conclude that the topological effects in the p sector are robust against changes in the electronic coupling and honeycomb period.

Table 2 | Coulomb energies.

ε_{in}	ε_{out}	U	V	Bandwidth	Absolute gap	Gap at Γ
14	14	48 meV	23 meV	20 meV	35 meV	56 meV
14	6	76 meV	43 meV			

On-site (U) and nearest-neighbor (V) Coulomb-interaction energies calculated for a honeycomb lattice of HgTe nanocrystals (with lattice parameters $q = 0.5$, $a = 5$ nm) compared with the width of the lowest p band, the absolute gap between the lowest p bands (the gap between band extrema) and the vertical gap at Γ ($k = 0$) between them. ε_{in} and ε_{out} are the dielectric constants of the materials composing the lattice (HgTe) and its environment, respectively.
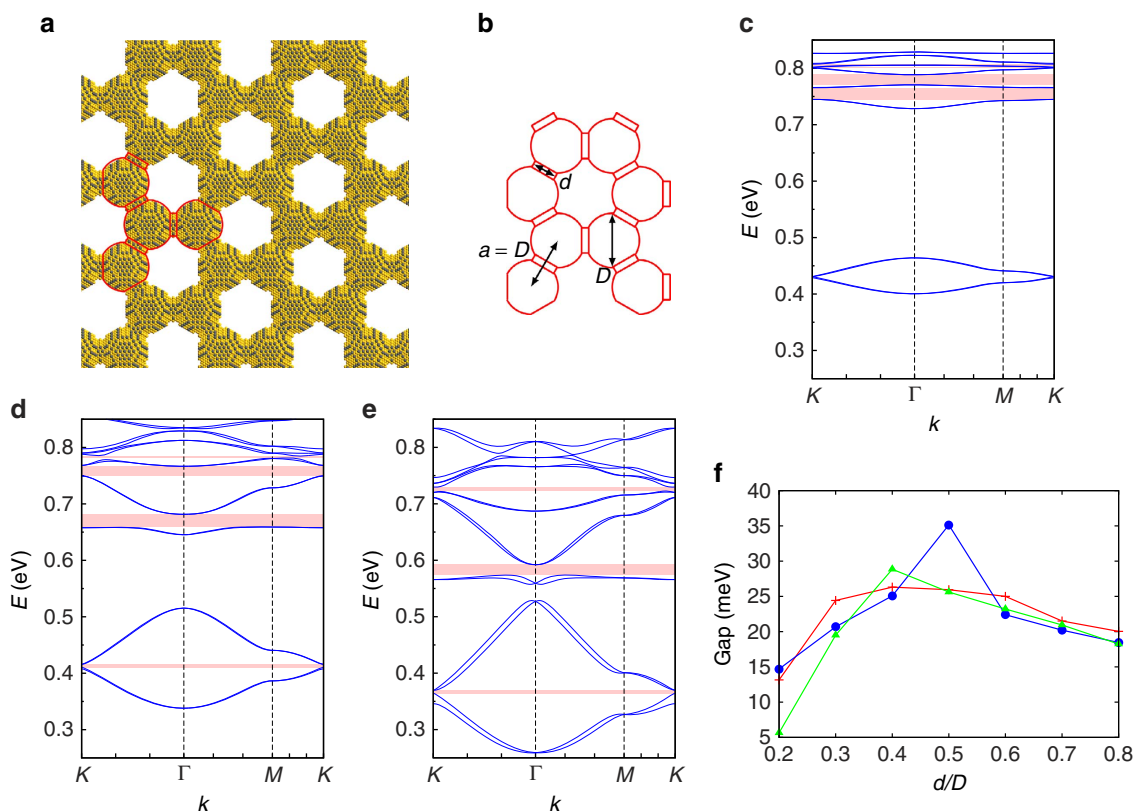
Figure 3 | Honeycomb lattice of HgTe spheres and its conduction band structure. (a,b) Top view of an assembly of spheres connected by cylinders, forming a honeycomb lattice of HgTe. Hg atoms are in yellow, Te atoms are in grey. The lattice spacing a, that is, the centre-to-centre distance between neighbour spheres, is equal to the diameter D of the spheres and d is the diameter of the cylinders. **(c–e)** Conduction band dispersions resulting from the atomistic TB calculation for $D = 5.0$ nm and $d/D = 0.3$ **(c)**, $d/D = 0.6$ **(d)** or $d/D = 0.8$ **(e)**. Non-trivial gaps are indicated by pink shaded regions. **(f)** Evolution of the gap between the lowest p bands versus d/D for three values of D (green triangles: $D = 5.9$ nm; blue circles: $D = 5.0$ nm; red crosses: $D = 4.1$ nm).

Discussion

In summary, we have performed atomistic TB calculations of the band structure of 2D honeycomb lattices of HgTe. We demonstrate that the strong SOC of HgTe combined with the honeycomb structure results in several topological phases. The calculated band structure can be described by a honeycomb lattice model as in graphene but including multi-orbital degrees of freedom that generate in particular a topologically non-trivial flat band. By taking advantage of these features, we show that in the same structure not only the QSHE, but potentially also the elusive fractional QSHE could be observed, just by varying the electron density. Both topological effects turn out to be protected by a gap as large as 35 meV, and can thus be observed at high temperatures. Honeycomb superlattices of HgTe are therefore platforms of high interest to study electrons on a multi-orbital honeycomb lattice under strong SOC. Such structures could be fabricated by nanocrystal self-assembly (in a similar way as for PbSe and CdSe[14,15]) or by a combination of gas-phase deposition and lithography. Our results open the path towards high-temperature quantum spintronics in artificial graphene.

Methods

Atomistic TB methodology. The electronic structure of HgTe superlattices is calculated within the TB approximation, as described in detail in ref. 38. The TB Hamiltonian matrix is written in a basis of atomic orbitals ($sp^3d^5s^*$ for each spin orientation) as function of parameters that have been obtained by fitting to two reference band structures: Close to the Fermi level, we use the $\mathbf{k} \cdot \mathbf{p}$ band structure of ref. 44, whereas elsewhere we use the band structure of ref. 45 obtained using a quasi-particle self-consistent GW approximation in a hybrid scheme. In the present work, we have used the TB parameters that give the band structure of HgTe at 300 K. The surfaces of the superlattices are saturated by pseudo-hydrogen atoms that push surface states far from the energy regions of interest in this study. Therefore surface states do not interfere with edge states predicted in ribbons. Owing to the large size of the systems that we have studied (up to $\approx 10^5$ atoms per unit cell), only near-gap eigenstates are calculated using the numerical methods described in ref. 46.

Calculation of the Z_2 topological invariant. The Z_2 topological invariant (spin Chern number C_s) for the bands of interest is calculated using the model Hamiltonian following the methodology proposed in ref. 47 and derived from ref. 48. This approach works even for systems without inversion symmetry, which is the case here. C_s is given by a sum of terms calculated on a regular lattice in the Brillouin zone. We have checked that the results converge for a mesh denser than 21×21 k vectors. In all cases, the invariants that we have computed for the bands are consistent with the number of edge states we observe in the bulk gaps.

Coulomb interactions. The Coulomb repulsion between electrons in honeycomb lattices of HgTe nanocrystals can be characterized as follows. For simplicity, we consider electrons in the s band, since in the case of individual nanocrystals, it was shown theoretically[49] and experimentally[50] that the Coulomb integrals are almost identical for states with s and p envelope functions. The Coulomb interaction associated to electrons on nanocrystals i and j is calculated as

$$\int |\Psi_i(\mathbf{r})|^2 \; |\Psi_j(\mathbf{r}')|^2 \; \mathcal{V}(\mathbf{r}, \mathbf{r}') d\mathbf{r} d\mathbf{r}' \qquad (4)$$

where $\Psi_i(\mathbf{r})$ is the s state on the nanocrystal i, and $\mathcal{V}(\mathbf{r}, \mathbf{r}')$ is the screened Coulomb energy of two interacting electrons at $\mathbf{r}$ and $\mathbf{r}'$. Taking into account that there is just one (spin degenerate) s state per nanocrystal, Ψ_i and Ψ_j are simply defined as the components on nanocrystals i and j of the wavefunction calculated for the lowest s band at Γ (or another k vector), normalized on their respective nanocrystals. Coulomb matrix elements are decomposed in the basis of the atomic orbitals and are calculated following the methodology described in ref. 51, by using usual approximations in the TB description, that is, neglecting overlaps between atomic orbitals and considering atomic charges as point-like charges. For the potential $\mathcal{V}$, we consider two configurations: First, a dielectrically homogeneous system, for which $\mathcal{V}(\mathbf{r}, \mathbf{r}') = e^2/(\varepsilon_{in}|\mathbf{r} - \mathbf{r}'|)$, where $\varepsilon_{in} = 14$ is the dielectric constant of HgTe; second, a dielectrically inhomogeneous system, for which $\mathcal{V}$ is calculated by solving the Poisson equation, with the dielectric constant inside (outside) the lattice equal to ε_{in} (ε_{out}). We have chosen $\varepsilon_{out} = 6$, a typical value taken to simulate the complex dielectric environment around semiconductor nanocrystals[49]. The on-site (U) and NN (V) terms are presented in Table 2. As expected, larger values are obtained for $\varepsilon_{out} = 6$ than for $\varepsilon_{out} = \varepsilon_{in}$. Longer-range Coulomb terms are expected to decay as the inverse of the distance between nanocrystals. However, it is important to note that these values do not take into account the extra screening induced by the electrons filling the bands. This could be computed, for example, in the random-

phase approximation, but this is clearly beyond the scope of the present work. Long-range interactions will be strongly screened, while short-range ones will be only slightly reduced[52]. In this context, for a band filling of the order of 1/3, correlations will be mainly governed by short-range effects.

References

1. Castro Neto, A. H., Guinea, F., Peres, N. M. R., Novoselov, K. S. & Geim, A. K. The electronic properties of graphene. *Rev. Mod. Phys.* **81,** 109–162 (2009).
2. Nair, R. R. *et al.* Fine structure constant defines visual transparency of graphene. *Science* **320,** 1308 (2008).
3. Katsnelson, M. I., Novoselov, K. S. & Geim, A. K. Chiral tunnelling and the Klein paradox in graphene. *Nat. Phys.* **2,** 620–625 (2006).
4. Novoselov, K. S. *et al.* Two-dimensional gas of massless Dirac fermions in graphene. *Nature* **438,** 197–200 (2005).
5. Du, X., Skachko, I., Duerr, F., Luican, A. & Andrei, E. Y. Fractional quantum Hall effect and insulating phase of Dirac electrons in graphene. *Nature* **462,** 192–195 (2009).
6. Bolotin, K. I., Ghahari, F., Shulman, M. D., Stormer, H. L. & Kim, P. Observation of the fractional quantum Hall effect in graphene. *Nature* **462,** 196–199 (2009).
7. Kane, C. L. & Mele, E. J. Quantum spin Hall effect in graphene. *Phys. Rev. Lett.* **95,** 226801 (2005).
8. Polini, M., Guinea, F., Lewenstein, M., Manoharan, H. C. & Pellegrini, V. Artificial honeycomb lattices for electrons, atoms and photons. *Nat. Nanotechnol* **8,** 625–633 (2013).
9. Soltan-Panahi, P. *et al.* Multi-component quantum gases in spin-dependent hexagonal lattices. *Nat. Phys.* **7,** 434–440 (2011).
10. Gomes, K. K., Mar, W., Ko, W., Guinea, F. & Manoharan, H. C. Designer Dirac fermions and topological phases in molecular graphene. *Nature* **483,** 306–310 (2012).
11. Wang, Z. F., Su, N. & Liu, F. Prediction of a two-dimensional organic topological insulator. *Nano Lett.* **13,** 2842–2845 (2013).
12. Gibertini, M. *et al.* Engineering artificial graphene in a two-dimensional electron gas. *Phys. Rev. B* **79,** 241406 (2009).
13. Park, C.-H. & Louie, S. G. Making massless Dirac fermions from a patterned two-dimensional electron gas. *Nano Lett.* **9,** 1793–1797 (2009).
14. Evers, W. H. *et al.* Low-dimensional semiconductor superlattices formed by geometric control over nanocrystal attachment. *Nano Lett.* **13,** 2317–2323 (2013).
15. Boneschanscher, M. P. *et al.* Long-range orientation and atomic attachment of nanocrystals in 2D honeycomb superlattices. *Science* **344,** 1377–1380 (2014).
16. Kalesaki, E. *et al.* Dirac cones, topological edge states, and nontrivial flat bands in two-dimensional semiconductors with a honeycomb nanogeometry. *Phys. Rev. X* **4,** 011010 (2014).
17. Zhang, G.-F., Li, Y. & Wu, C. Honeycomb lattice with multiorbital structure: topological and quantum anomalous Hall insulators with large gaps. *Phys. Rev. B* **90,** 075114 (2014).
18. Haldane, F. D. M. Model for a quantum Hall effect without Landau levels: condensed-matter realization of the "parity anomaly". *Phys. Rev. Lett.* **61,** 2015–2018 (1988).
19. Wu, C., Bergman, D., Balents, L. & Das Sarma, S. Flat bands and Wigner crystallization in the honeycomb optical lattice. *Phys. Rev. Lett.* **99,** 070401 (2007).
20. Sun, K., Gu, Z., Katsura, H. & Das Sarma, S. Nearly flatbands with nontrivial topology. *Phys. Rev. Lett.* **106,** 236803 (2011).
21. Venderbos, J. W. F., Daghofer, M. & van den Brink, J. Narrowing of topological bands due to electronic orbital degrees of freedom. *Phys. Rev. Lett.* **107,** 116401 (2011).
22. Yang, S., Gu, Z.-C., Sun, K. & Das Sarma, S. Topological flat band models with arbitrary Chern numbers. *Phys. Rev. B* **86,** 241112 (2012).
23. Ölschläger, M. *et al.* Interaction-induced chiral $p_x \pm i p_y$ superfluid order of bosons in an optical lattice. *New J. Phys.* **15,** 083041 (2013).
24. Neupert, T., Santos, L., Chamon, C. & Mudry, C. Fractional quantum Hall states at zero magnetic field. *Phys. Rev. Lett.* **106,** 236804 (2011).
25. Hu, X., Kargarian, M. & Fiete, G. A. Topological insulators and fractional quantum Hall effect on the ruby lattice. *Phys. Rev. B* **84,** 155116 (2011).
26. Goerbig, M. O. From fractional Chern insulators to a fractional quantum spin Hall effect. *Eur. Phys. J. B* **85,** 1–8 (2012).
27. Regnault, N. & Bernevig, B. A. Fractional Chern insulator. *Phys. Rev. X* **1,** 021014 (2011).
28. Tang, E., Mei, J.-W. & Wen, X.-G. High-temperature fractional quantum Hall states. *Phys. Rev. Lett.* **106,** 236802 (2011).
29. Xiao, D., Zhu, W., Ran, Y., Nagaosa, N. & Okamoto, S. Interface engineering of quantum Hall effects in digital transition metal oxide heterostructures. *Nat. Commun.* **2,** 596 (2011).

30. He, J., Wang, B. & Kou, S.-P. Ferromagnetism and antiferromagnetism of a correlated topological insulator with a flat band. *Phys. Rev. B* **86,** 235146 (2012).

31. Bergholtz, E. J. & Liu, Z. Topological flat band models and fractional Chern insulators. *Int. J. Mod. Phys. B* **27,** 1330017 (2013).

32. Bernevig, B. A., Hughes, T. L. & Zhang, S.-C. Quantum spin Hall effect and topological phase transition in HgTe quantum wells. *Science* **314,** 1757–1761 (2006).

33. König, M. *et al.* Quantum spin Hall insulator state in HgTe quantum wells. *Science* **318,** 766–770 (2007).

34. Ran, Y., Zhang, Y. & Vishwanath, A. One-dimensional topologically protected modes in topological insulators with lattice dislocations. *Nat. Phys.* **5,** 298–303 (2009).

35. Juričić, V., Mesaros, A., Slager, R.-J. & Zaanen, J. Universal probes of two-dimensional topological insulators: dislocation and π flux. *Phys. Rev. Lett.* **108,** 106403 (2012).

36. Rüegg, A. & Lin, C. Bound states of conical singularities in graphene-based topological insulators. *Phys. Rev. Lett.* **110,** 046401 (2013).

37. Slager, R.-J., Mesaros, A., Juričić, V. & Zaanen, J. The space group classification of topological band-insulators. *Nat. Phys.* **9,** 98–102 (2013).

38. Allan, G. & Delerue, C. Tight-binding calculations of the optical properties of HgTe nanocrystals. *Phys. Rev. B* **86,** 165437 (2012).

39. Ye, J. T. *et al.* Liquid-gated interface superconductivity on an atomically flat film. *Nat. Mater.* **9,** 125–128 (2010).

40. Germeau, A. *et al.* Optical transitions in artificial few-electron atoms strongly confined inside ZnO nanocrystals. *Phys. Rev. Lett.* **90,** 097401 (2003).

41. Beugeling, W., Goldman, N. & Morais Smith, C. Topological phases in a two-dimensional lattice: magnetic field versus spin-orbit coupling. *Phys. Rev. B* **86,** 075118 (2012).

42. Slater, J. C. & Koster, G. F. Simplified LCAO method for the periodic potential problem. *Phys. Rev.* **94,** 1498–1524 (1954).

43. Kourtis, S., Neupert, T., Chamon, C. & Mudry, C. Fractional Chern insulators with strong interactions that far exceed band gaps. *Phys. Rev. Lett.* **112,** 126806 (2014).

44. Man, P. & Pan, D. S. Infrared absorption in HgTe. *Phys. Rev. B* **44,** 8745–8758 (1991).

45. Svane, A. *et al.* Quasiparticle band structures of β-HgS, HgSe, and HgTe. *Phys. Rev. B* **84,** 205205 (2011).

46. Niquet, Y. M., Delerue, C., Allan, G. & Lannoo, M. Method for tight-binding parametrization: Application to silicon nanostructures. *Phys. Rev. B* **62,** 5109–5116 (2000).

47. Fukui, T. & Hatsugai, Y. Quantum spin Hall effect in three dimensional materials: Lattice computation of Z_2 topological invariants and its application to Bi and Sb. *J. Phys. Soc. Jpn* **76,** 053702 (2007).

48. Fu, L. & Kane, C. L. Time reversal polarization and a Z_2 adiabatic spin pump. *Phys. Rev. B* **74,** 195312 (2006).

49. Niquet, Y. M., Delerue, C., Allan, G. & Lannoo, M. Interpretation and theory of tunneling experiments on single nanostructures. *Phys. Rev. B* **65,** 165334 (2002).

50. Banin, U., Cao, Y., Katz, D. & Millo, O. Identification of atomic-like electronic states in indium arsenide nanocrystal quantum dots. *Nature* **400,** 542–544 (1999).

51. Delerue, C., Lannoo, M. & Allan, G. Calculations of the electron-energy-loss spectra of silicon nanostructures and porous silicon. *Phys. Rev. B* **56,** 15306–15313 (1997).

52. Nozières, P. & Pines, D. *Theory Of Quantum Liquids* (Westview Press, 1999).

Acknowledgements

Author contributions

W.B., E.K. and C.D. performed the calculations. Y.-M.N. contributed to the development of the codes and methodologies. C.D., D.V. and C.M.S. supervised the project. All authors were involved in writing of the manuscript.

Additional information

Supplementary Information accompanies this paper at http://www.nature.com/naturecommunications

Competing financial interests: The authors declare no competing financial interests.

Reprints and permission information is available online at http://npg.nature.com/reprintsandpermissions/

How to cite this article: Beugeling, W. *et al.* Topological states in multi-orbital HgTe honeycomb lattices. *Nat. Commun.* 6:6316 doi: 10.1038/ncomms7316 (2015).